



JOINT INSTITUTE FOR NUCLEAR RESEARCH  
Frank Laboratory of Neutron Physics

# FINAL REPORT ON THE START PROGRAMME

*Investigation of the feasibility of creating a  
compound polarizer from CoFe crystals to  
increase the intensity of a polarized neutron  
beam*

**Supervisor:**

Dr. Natalia Viktorovna Rebrova  
Dr. Valery Leonidovich Kuznetsov

**Student:**

Riabykh Egor, Voronezh State  
University

**Participation period:**

February 15 – April 4,  
Winter Session 2026

Dubna, 2026

# Contents

Abstract.....	3
Introduction.....	3
1. Polarization of neutrons by the diffraction method .....	8
2. Pulsed neutron source IBR-2M.....	6
3. The "Kolchida" setup .....	7
4. CoFe single crystals.....	8
5. Determination of single crystals mosaicity .....	9
6. Determination of the energy and wavelength of diffracted neutrons by the time-of-flight method .....	11
7. Fabrication of a compound polarizer from two CoFe single crystals	
7.1. Use of the first and second single crystals.....	13
7.2. Use of the first and third single crystals .....	15
8. Attenuation of the diffracted neutron beam intensity upon passing through a CoFe crystal .....	17
Conclusion .....	18
Acknowledgements .....	18
References.....	19

## Abstract

This work investigates the feasibility of a compound neutron polarizer made of several Co(92%)–Fe(8%) alloy single crystals to increase the intensity of polarized neutrons. Experiments were carried out at the IBR-2M pulsed reactor using the “Kolchida” spectrometer. The mosaic spreads of three crystals were determined, rocking curves of individual crystals and their assemblies were studied, and time-of-flight spectra of diffracted neutrons were measured. It is shown that in Laue geometry, the sequential arrangement of crystals leads to beam attenuation that outweighs the gain from mosaicity. Nevertheless, the fundamental feasibility of increasing the neutron flux intensity by assembling crystals into a stack has been demonstrated.

## Introduction

This work examines the fundamental feasibility of creating a compound neutron polarizer from several CoFe alloy single crystals in order to increase the intensity of polarized neutrons.

Polarized neutrons are used in experimental searches for P-odd angular correlations of gamma-ray emission in  $(n,\gamma)$  reactions [1]. Effects associated with the violation of spatial parity in nuclei are strongly enhanced near p-wave neutron resonances. Increasing the neutron flux would allow measurements with higher precision.

The “Kolchida” spectrometer [2] can be used for conducting such experiments. Polarization of slow neutron beams on this setup is achieved by the diffraction method in transmission geometry (Laue geometry). The neutron beam passes through a CoFe single crystal polarized by an external magnetic field and is reflected from the (200) planes. The reflected neutron beam turns out to be both polarized and monochromatic.

The idea of a compound neutron polarizer appears to have been first proposed in [3]. In that paper, a polarized neutron beam with a wavelength of 1.37 Å was obtained by reflection from the (200) planes of a CoFe single crystal in Bragg geometry. The authors present the main methods for increasing the intensity of a polarized neutron beam:

1. Increasing the thickness of the crystal;
2. Increasing the mosaic spread of the crystal;
3. Using a multiple crystal.

The standard single-crystal holders of the “Kolchida” setup are not designed to hold several crystals simultaneously in an external magnetic field. Therefore, within the framework of this work, measurements were carried out in the absence of guiding magnetic fields.

During the work, the mosaic spreads of three CoFe alloy crystals, the energy and wavelength of the diffracted neutrons were determined, and the rocking curves of several compound polarizer assemblies were analyzed.

Analysis and visualization of experimental data were performed using the “Origin” software [4]; calculations were carried out using “Wolfram Mathematica” [5]. Additionally, programs described in the following sections were used to control the setup and acquire spectra.

# 1. Polarization of neutrons by the diffraction method

The theory of the method is described in the book [6].

The interaction of thermal neutrons with atoms of a ferromagnetic substance consists of two parts. The first part is the nuclear interaction between the neutron and the nucleus. This, in turn, consists of neutron scattering and radiative capture. Scattering of thermal neutrons by nuclei can be coherent and incoherent. Coherence is associated with the constancy of phase relationships between waves coming from different scattering centers.

The second part of the interaction of a neutron with atoms of a ferromagnetic substance is the interaction of the neutron with the magnetic moment of the atom. From the theory of ferromagnetism, it is known that the magnetic moments of electrons responsible for ferromagnetic properties are strongly coupled to each other. The resultant magnetic moments of atoms in a single domain are oriented parallel to a certain direction. However, the directions of spontaneous magnetization of individual domains are not correlated with each other in an unmagnetized ferromagnet. When approaching saturation of the ferromagnet, the magnetization directions of individual domains tend to become parallel to the direction of the external magnetic field. The regularity of the arrangement of atoms in the ferromagnet and the orientation of the atomic magnetic moments cause the magnetic scattering of neutrons by atoms of the ferromagnet in a state close to saturation to be coherent.

The amplitude of coherent magnetic scattering  $a_m$  is analogous to the amplitude of coherent nuclear scattering  $a_N$ . Nuclear and magnetic scattering interfere with each other. In this case, the amplitude of the process is:

$$a = a_N + a_m, \quad (1.1)$$

The magnetic scattering amplitude is defined as  $a_m = p(\mathbf{q}\boldsymbol{\lambda})$ . Here,  $\mathbf{q}$  – is the magnetic interaction vector,  $\boldsymbol{\lambda}$  – is a unit vector directed along the neutron spin (polarization vector);  $p = r_0\mu_n S f$ , where  $r_0 = e^2/mc^2$  – is the classical electron radius,  $\mu_n$  – is the neutron magnetic moment in nuclear magnetons,  $S$  – is the spin quantum number of the scattering atom in units of  $\hbar$ ,  $f$  – is the atomic magnetic form factor.

If the incident and diffracted beams lie in a plane perpendicular to the direction of magnetization of the crystal, then the cross sections for the two neutron spin states (identified as «+» for the spin parallel to, and «-» for the spin opposite to, the applied magnetic field) can be written as

$$\sigma_+ = 4\pi(a_N + p)^2 \quad (1.2)$$

and

$$\sigma_- = 4\pi(a_N - p)^2 \quad (1.3)$$

There are two methods for mounting single crystals: transmission (Laue geometry) and reflection (Bragg geometry). In the first method, the diffracted beam passes through the entire thickness of the crystal and exits on the side opposite to the incident beam. In the second, the diffracted beam exits the crystal on the same side as the incident beam. If the atomic reflecting planes are parallel to the surface of a plane-parallel single crystal or make a right angle with this plane, then the neutron beams incident on and diffracted from the crystal make equal angles with the crystal surface. Such cases are called symmetric diffraction.

From a given family of planes ( $hkl$ ) with interplanar spacing  $d_{hkl}$  for a given glancing angle  $\theta$  only those neutrons whose wavelengths  $\lambda$  satisfy the Wulff–Bragg condition will be reflected:

$$n\lambda = 2d_{hkl}\sin(\theta), \quad (1.4)$$

where  $n$  – is a positive integer called the order of reflection. This condition makes it possible to selectively reflect neutrons with a specific wavelength, which is used for beam monochromatization.

The integrated intensity of the diffracted neutron beam is given by the expression

$$I = R\Phi_0, \quad (1.5)$$

where  $R$  – is the integrated reflectivity;  $\Phi_0 = \int J_0(\varepsilon)d\varepsilon$  – is the flux of incident neutrons integrated over the cross-section of the neutron beam intercepted by the crystal,  $J_0(\varepsilon)$  – is the intensity of incident neutrons per unit interval of the parameter  $\varepsilon$ . The parameter  $\varepsilon$  can be the wavelength or the glancing angle of the neutrons incident on the crystal. The quantities

$$R^\theta = \int \frac{\Phi}{\Phi_0} d(\theta - \theta_B), \quad (1.6)$$

$$R^\lambda = \int \frac{\Phi}{\Phi_0} d(\lambda - \lambda_B), \quad (1.7)$$

are related by

$$R^\lambda = R^\theta 2d_{hkl} \cos\theta, \quad (1.8)$$

where  $\Phi$  – is the flux of diffracted neutrons.

For the model of an ideally imperfect crystal in Laue geometry with symmetric diffraction in the thin-crystal approximation, we can obtain for  $R^\theta$ :

$$R^\theta = \frac{Qt_0}{\gamma_0} \exp\left\{-\mu \frac{t_0}{\gamma_0}\right\}, \quad (1.9)$$

where  $\mu$  – is the linear neutron absorption coefficient,  $t_0$  – is the thickness of the crystal,  $\gamma_0 = \sin\theta_B$  – is the direction cosine of the incident neutrons, and

$$Q = \frac{\lambda^3 |F|^2}{|V_c|^2 \sin(2\theta_B)},$$

where  $V_c$  – is the volume of the unit cell of the crystal, and  $F$  – is the structure factor.

## 2. Pulsed neutron source IBR-2M

The IBR-2M reactor, operating at the Frank Laboratory of Neutron Physics of the Joint Institute for Nuclear Research, is a pulsed research nuclear reactor with fast neutrons and a compact core. Figure 1 shows a schematic diagram of the reactor.

The reactor parameters are as follows [7]: average power – 1.5 MW, maximum fuel burnup – 9%, rotation frequency of the main movable reflector – 600 rpm, rotation frequency of the auxiliary movable reflector – 300 rpm. Power pulses are generated at a frequency of 5 Hz by reactivity modulators: the main movable reflector (MMR) and the auxiliary movable reflector (AMR). When both reflectors approach the core, a power pulse occurs. The most important characteristic of IBR-2M is the power pulse shape, which is well approximated by a Gaussian distribution with a full width at half maximum of  $200 \pm 4 \mu\text{s}$ .

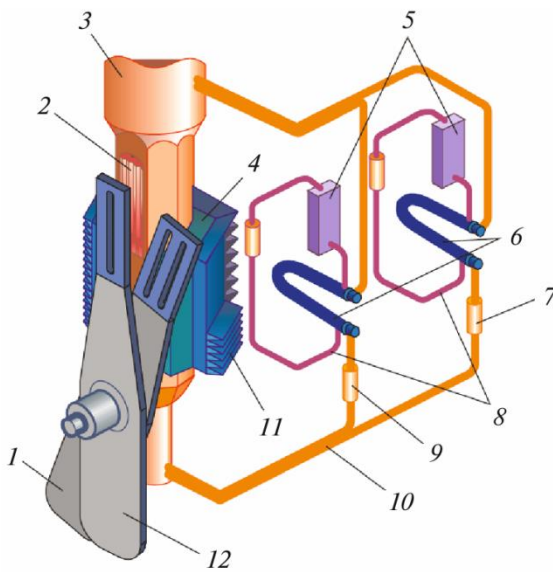


Figure 1. Schematic diagram of the IBR-2M reactor with movable reflector blades: (1) main movable reflector; (2) core; (3) reactor vessel; (4) stationary reflectors; (5) air-sodium heat exchangers; (6) intermediate heat exchangers; (7) sodium pump; (8) secondary cooling circuit; (9) sodium pump; (10) primary cooling circuit; (11) moderator; (12) additional movable reflector.

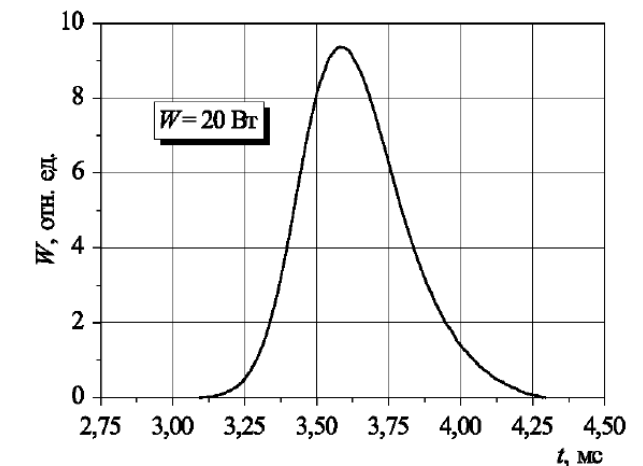


Figure 2. The shape of the thermal neutron power pulse near the surface of the IBR-2M reactor moderator [8]

### 3. The "Kolchida" setup

The "KOLCHIDA" polarized neutron spectrometer is located at tangential channel No. 1 of the IBR-2M pulsed reactor. A general scheme of the setup is shown in Figure 3.

The formation of the neutron spectrum takes place in the reactor moderator. Neutrons emerging from the moderator pass through a channel in the biological shield, in which three collimators are installed, providing an angular divergence of the neutron beam at the exit equal to

$$\alpha = \frac{0,05 \text{ m}}{12,4 \text{ m}} \approx 0,0040323 \text{ radian} \approx 13'52'' \quad (3.1)$$

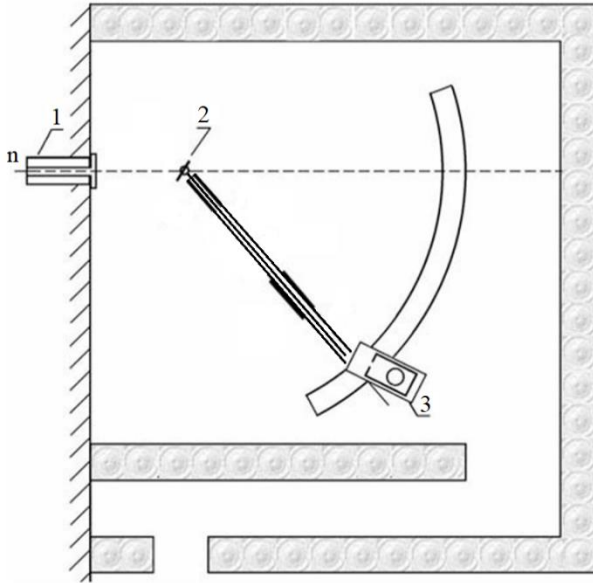


Figure 3. General diagram of the setup: 1 – collimator window; 2 – polarizer crystal; 3 – detector.

In this work, the white neutron beam was diffracted by single crystals of the Co(92%)–Fe(8%) alloy. The crystals were sequentially fixed in a holder, which was then placed in the position of polarizer 2.

The spectrometer is mounted on a metal support, along which a massive arm moves. The axis around which the arm rotates coincides with the rotation axis of polarizer 2.

A platform for the neutron detector 3 is mounted on the arm. The setup provides rotation and measurement of rotations around the vertical axes of the polarizer crystal, the arm, and the detector platform. Rotation of the setup components was provided by stepper motors; rotation angle control was provided by sensors [9]. All rotations are independent of each other and allow angles to be set with an accuracy of about 3 arcminutes. The programs

"MOTOR adjust" and "SENSOR adjust" were used to control the stepper motors and to read the sensor data.

The readings of the angular sensor in the "zero" position, indicated by the dashed line in the figure, are as follows: detector –  $296^{\circ}36'$ , spectrometer arm –  $328^{\circ}43'$ . Neutron diffraction measurements were performed for an incidence angle  $\theta = 18^{\circ}20'$  with the angular sensor readings of  $296^{\circ}36'$  for the detector and  $292^{\circ}03'$  for the spectrometer arm.

An «SNM»-17 counter, filled with  $^3\text{He}$  to a pressure of 10 serves as the neutron detector. The vertically placed counter is housed in a box made of borated polyethylene, lined on the inside with cadmium to reduce background. The entrance window of the detector has a size of 10 mm horizontally and a height of 50 mm.

The flight-path distance from the moderator at the reactor core to the detector is 15.9 m and includes the following distances: moderator–polarizer 12.4 m, polarizer–detector 3.5 m. Biological shielding made of concrete blocks has been built for the spectrometer. Access to the setup is through a labyrinth.

## 4. CoFe single crystals

As mentioned above, three single crystals of the Co(92%)–Fe(8%) alloy were used in this work. The dimensions of the crystals are given in Table 1. The diffracted neutron beam was obtained using reflection from the (200) planes in transmission geometry. The crystals were grown, processed, and tested in Poland, at the Institute of Nuclear Research (Swierk) [2].

Pure cobalt has a hexagonal structure. Its magnetization requires the application of strong magnetic fields. The addition of 8 at.% iron stabilizes the cubic face-centered phase of cobalt. The cubic phase of cobalt is relatively easy to magnetize. The magnetic and nuclear unit cells coincide with each other.

The interplanar distances  $d_{hkl}$  are calculated using the formula

$$\frac{1}{d^2} = \frac{(h^2 + k^2 + l^2)}{a^2}. \quad (4.1)$$

where  $a = 3,53 \text{ \AA}$  – is the lattice constant of the Co(92%)-Fe(8%) alloy.

Thus, for the (200) planes we have:  $2d_{200} = 3,53 \text{ \AA}$ .

Table 1. The dimensions of the single crystals [9]

Single crystal	Length, mm	Width, mm	Thickness, mm
№1	34	31	3
№2	42	33	1
№3	53	33	3

The nuclear scattering length of cobalt is  $a_N(\text{Co}) = 0.28 \cdot 10^{-12} \text{ cm}$ , so the average nuclear scattering length of the alloy is

$$a_N = 0.92a_N(\text{Co}) + 0.08a_N(\text{Fe}) \approx 0.33 \cdot 10^{-12} \text{ cm}.$$

The magnetic scattering length of the alloy is approximately  $p \approx 0.47 \cdot 10^{-12} f \text{ cm}$ , where  $f$  is the atomic magnetic form factor. For the (200) reflection:

Table 2. Magnetic form factor for face-centered cobalt

(hkl)	$\sin\theta/\lambda$	$F_m/F_N$	$f$
(200)	0.244	$1.21 \pm 0.06$	$0.781 \pm 0.040$

We obtain  $p = 0.31 \cdot 10^{-12} \text{ cm}$ , i.e., this reflection should provide almost complete polarization of the neutrons.

Since orientation effects are significant for the single crystals used in this work, for all three single crystals the A/B sides and the "up-down", "left-right" orientation were marked [9]. The crystal marking scheme is shown in Figure 4.

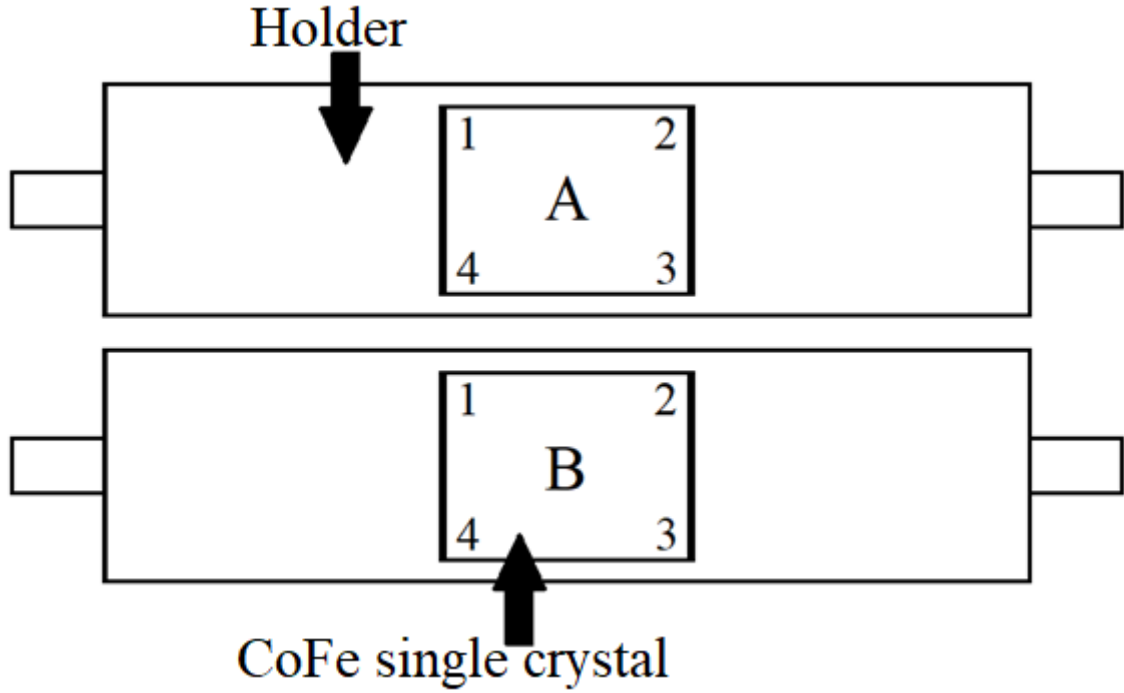


Figure 4. Marking of the single crystals.

## 5. Determination of single crystals mosaicity

According to the above-mentioned model of an ideally imperfect crystal, we assume that the crystal consists of individual mosaic blocks possessing an ideal structure, but of such small dimensions that extinction for an individual block can be neglected [6].

Assume that the mosaic blocks have a rectangular shape, and the surfaces of individual blocks do not lie in the same plane. The angular distribution of the normals to the block surfaces is given by a Gaussian function

$$W(\Delta) = \frac{1}{\eta\sqrt{2\pi}} \exp\left\{-\frac{\Delta^2}{2\eta^2}\right\}, \quad (5.1)$$

where  $\eta$  is the mosaic spread,  $W(\Delta)d\Delta$  – is the fraction of mosaic blocks in the angular interval from  $\Delta$  to  $\Delta + d\Delta$ .

The Bragg–Wulff angle  $\theta_B$  is defined with respect to the position of the crystallographic plane. For a direction corresponding to the glancing angle  $\theta_B$ , the crystal mosaicity allows other glancing angles  $\theta$  to occur, with the difference  $\Delta = \theta_B - \theta$  being determined by distribution (5.1).

For each CoFe single crystal, a rocking curve – the dependence of the reflected neutron intensity on the glancing angle – was measured. The measurement time for each point was 20 seconds, the step between positions was  $6' = 0,00174532$  rad, and the instrument readings of the angular sensors were taken as the abscissa axis. The rocking curves were approximated by a Gaussian function.

The full width at half maximum  $\beta$  depends on the mosaic spread  $\eta$  of the investigated single crystal and the angular divergence  $\alpha$  of the incident neutron beam  $\alpha$  as follows

$$\beta^2 = \alpha^2 + \eta^2, \quad (5.2)$$

whence

$$\eta = \sqrt{\beta^2 - \alpha^2}. \quad (5.3)$$

The error  $\sigma_\eta$  is equal to

$$\sigma_\eta = \frac{d\beta}{d\eta} \sigma_\beta, \quad \sigma_\beta = \sqrt{\sigma_{stat} + \sigma_{inst}}, \quad (5.4)$$

where  $\sigma_{stat}$  – is the standard error for the fit, automatically calculated by the program, and  $\sigma_{inst}$  is the error due to backlash..

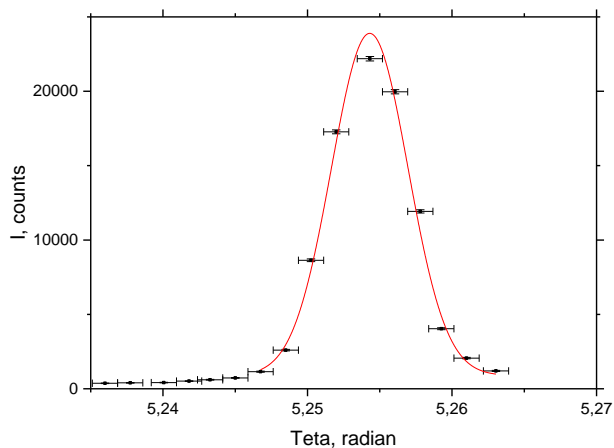


Figure 5. Rocking curve of crystal 1, side A41 facing the reactor. Red line – fit by a Gaussian function.

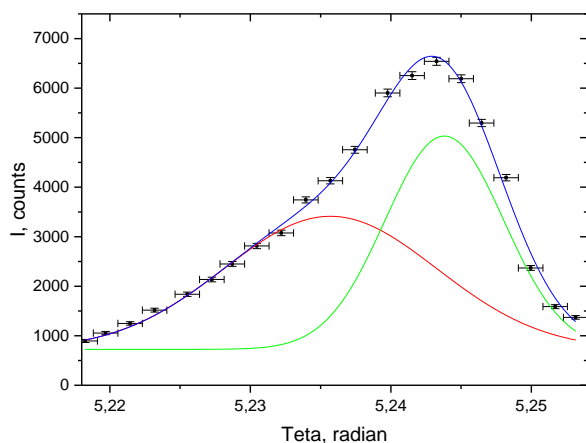


Figure 6. Rocking curve for crystal 2, with side A12 facing the reactor. The red line is the Gaussian fit for the first mosaic domain, the green line is for the second. The blue line is the total fit.

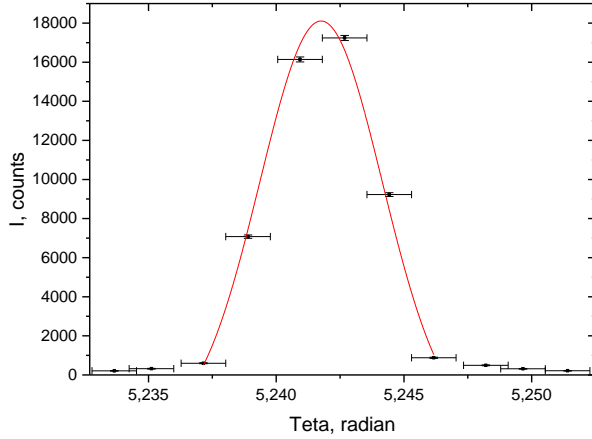


Figure 7. Rocking curve of crystal 3, with side A12 facing the reactor. The red line is the Gaussian fit.

During the analysis, it was found that the second crystal is a twin, i.e., it contains two scattering domains. Taking this into account, the following crystal mosaicities were obtained:

Table 3. Mosaicity of single crystals

Single crystal	Mosaicity $\eta$ , radian	Mosaicity $\eta$ , minutes
1	$0.00476219 \pm 0.00119937$	$16' \pm 04'$
2, 1 domain	$0.01737833 \pm 0.00863892$	$59' \pm 29'$
2, 2 domain	$0.00906351 \pm 0.00213051$	$31' \pm 07'$
3	$0.00394341 \pm 0.00155986$	$13' \pm 05'$

Also, for the crystals, the glancing angles at which the maximum intensity of the diffracted neutron beam can be observed according to the angular sensor of the polarizer stepper motor, were obtained:

Table 4. Glancing angles for each crystal at which the intensity maximum is observed. The values were obtained from the fit functions

Single crystal	$\theta$ , radian	$\theta$ , degree	I, counts
N <sub>o</sub> 1	$5.25431 \pm 0.00087$	$301^{\circ} 3' \pm 3'$	$23893 \pm 154$
N <sub>o</sub> 2	$5.24291 \pm 0.00087$	$300^{\circ} 24' \pm 3'$	$6643 \pm 81$
N <sub>o</sub> 3	$5.24176 \pm 0.00087$	$300^{\circ} 20' \pm 3'$	$18106 \pm 134$

## 6. Determination of the energy and wavelength of diffracted neutrons by the time-of-flight method

In this work, the neutron energy, the corresponding wavelength, and the angle  $\theta$  were determined for crystals 1 and 3. The channel width in the measurement of the first crystal was 10  $\mu$ s, and in the measurement of the second – 3.2  $\mu$ s. The measurement time for both spectra was 10 min.

When analyzing the data, the peaks were approximated using the Asym2Sig function from the "Origin" program with a linear background. This function was chosen because, at high event counts, the deviation of the peak shape from a normal distribution could no longer be neglected.

The time-of-flight method was used to determine the energy and wavelength of the diffracted neutrons. The neutron energy  $E_n$  (eV) is determined from the expression:

$$E_n = \left( \frac{72,3 \cdot L}{\tau} \right)^2, \quad (6.1)$$

where  $L = 15.4$  (m) is the flight-path length,  $\tau = t - t_0$  ( $\mu$ s) is the flight time,  $t_0$  is the moment when the neutron crosses the beginning of the flight-path, and  $t$  is the moment when the neutron reaches the detector.  $t_0$  is determined by the start signal and corresponds to the peak of the reactor power pulse, and  $t$  corresponds to the peak of the diffraction order under consideration (Fig. 8).

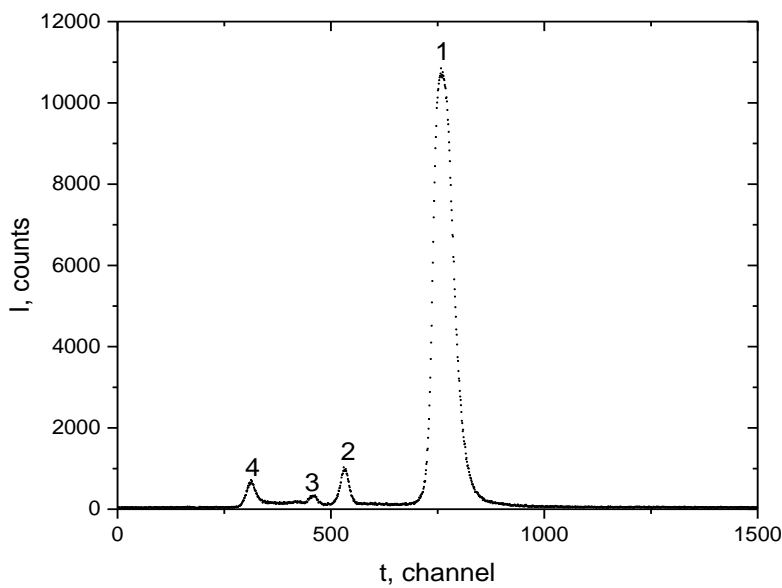


Figure 8. Instrumental time-of-flight spectrum. 1, 2, 3 – first, second and third diffraction orders. 4 – reactor power pulse.

The relationship between neutron energy and wavelength is

$$\lambda = \frac{h}{\sqrt{2m_n E_n}}, \quad (6.2)$$

or, after substituting the constants,

$$\lambda = \frac{0,286}{\sqrt{E_n}}, \quad (6.3)$$

where  $\lambda$  is the wavelength in  $\text{\AA}$ ,  $E_n$  is the neutron energy in eV.

The angle  $\theta_B$  for each diffraction order was found using formula (1.4). Then, taking into account the errors, a weighted average value was calculated for it.

The uncertainty in the neutron flight time  $\Delta t = \sqrt{\Delta t_n^2 + \Delta t_{ch}^2 + \Delta t_d^2}$  consists of the uncertainties of the neutron pulse duration of the facility  $\Delta t_n$ , the width of the encoder time channel  $\Delta t_{ch}$  and the spread in event registration times in the detector  $\Delta t_d$ . When analyzing the experimental data in our case, the largest influence comes from the uncertainty of the power pulse duration, so the contributions of the others were neglected. The errors in energy, wavelength, and angles were found using an algorithm similar to formula (5.4). The uncertainty in flight time was taken as  $\Delta L = 0,01$  m.

Table 5. Results of time-of-flight spectra processing. Energy and wavelength are taken for the first order of diffraction

Single crystal	$\theta_B$ , degree	$E_n$ , meV	$\lambda$ , Å
№1	$18^\circ 29' \pm 16'$	$65.24 \pm 1.83$	$1.1197 \pm 0.0157$
№3	$18^\circ 32' \pm 16'$	$64.91 \pm 1.89$	$1.1226 \pm 0.0164$

The obtained values of the angle  $\theta_B$  are in agreement within the error with the known incidence angle  $\theta = 18^\circ 20'$ , which is equal to half the rotation angle of the spectrometer arm  $2\theta$ .

## 7. Fabrication of a compound polarizer from two CoFe single crystals

### 7.1. Use of the first and second single crystals

Each crystal is provided with its own separate holder. It is impossible to mount two holders on the rotating platform simultaneously. Therefore, we fixed all crystals in a single holder.

Due to the high mosaicity of the second crystal, the first measurement already showed an overlap of the rocking curves:

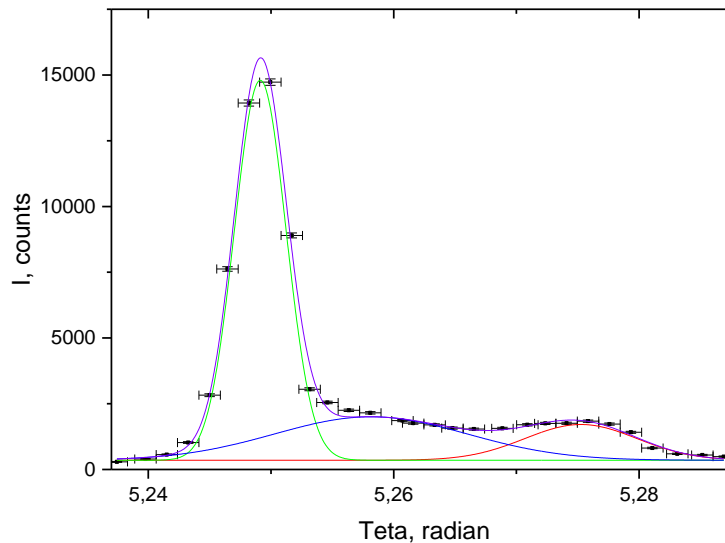


Figure 9. Facing the reactor: 1st crystal with side A41, then 2nd crystal with side A12. Green line – fit for the peak of the 1st crystal, blue – first domain of the 2nd crystal, red – second domain of the 2nd crystal. Violet line is the total fit.

Here, the 2nd crystal was placed in its "native" holder, and the first crystal was placed on top of it. As can be seen from the figure, the total intensity obtained was lower than that of the first crystal alone.

Next, we separated the peaks by tilting the first crystal by small angles using shims of various thicknesses, and then recorded rocking curves. The results are shown in Figure 10.

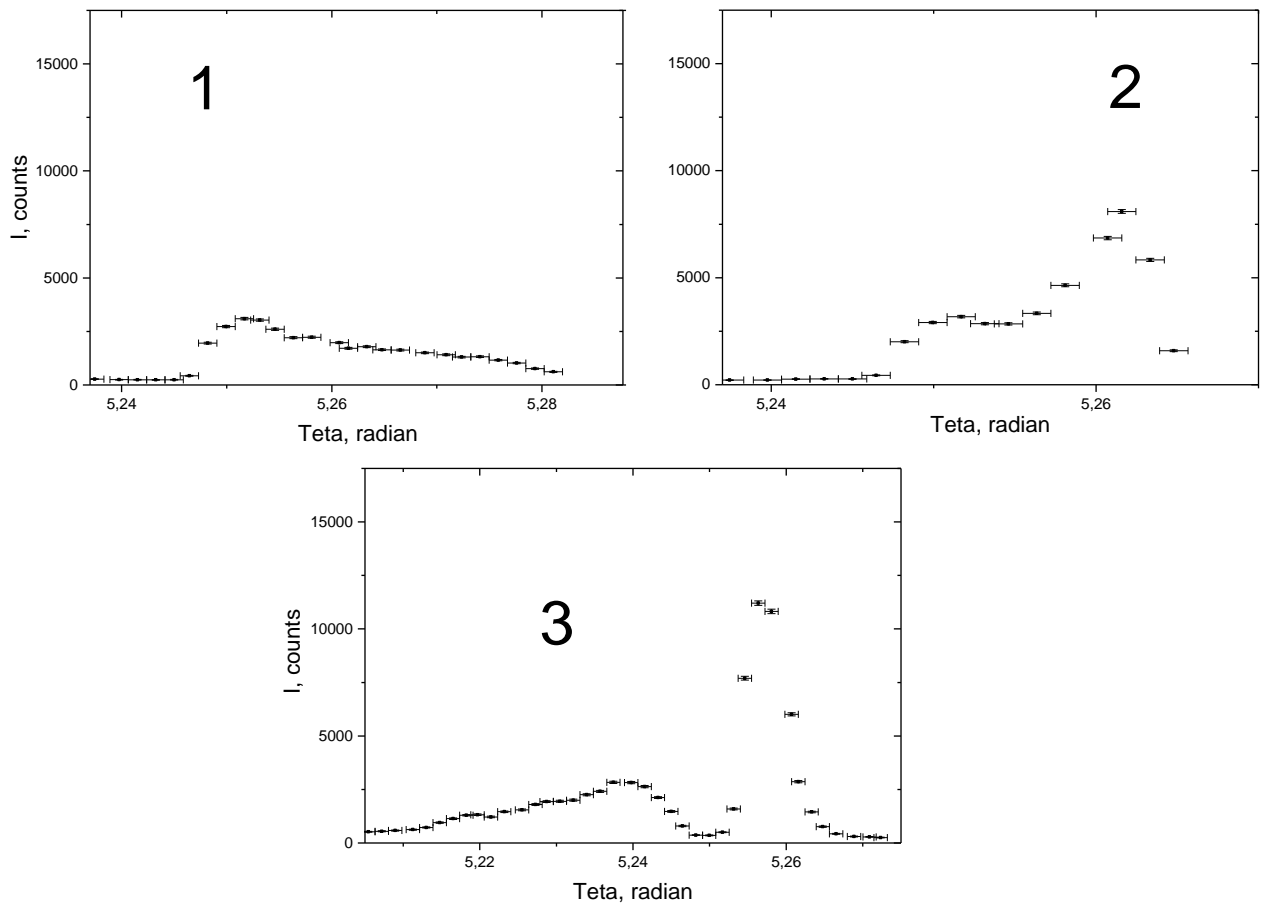


Figure 10. Facing the reactor:

- 1 – 1st crystal with side A41, then 2nd crystal with side A12. The first crystal was rotated to the right relative to the reactor by an angle of  $\approx 0.040$  radian;
- 2 – 1st crystal with side A41, then 2nd crystal with side A12. The first crystal was rotated to the left relative to the reactor by an angle of  $\approx 0.040$  radian;
- 3 – 2nd crystal with side B34, then 1st crystal with side B14. The assembly was rotated by 180 degrees relative to the previous position.

In graph 1, we shifted the peak position of the first crystal beyond the scanning range. In graph 2, a peak of the first crystal is visible. The reduced intensity compared to Figure 9 is explained by a slight deviation from the vertical position. In graph 3, after rotating the assembly by 180 degrees, we obtained two separated peaks. Their intensities dropped by a factor of two compared to the values measured for the individual crystals.

## 7.2. Use of the first and third single crystals

The second crystal is much more mosaic than the first and third. Therefore, it was more difficult to obtain merged reflections from the first and third crystals.

Figure 11 shows the results of scanning the crystal assembly in two positions. The second position differs from the first only by a 180° rotation of the assembly. The third crystal was placed in its "native" holder, and then the first crystal was fixed on top of it. From the recorded curves, it can be seen that the position of the reflection of the first crystal mirrored relative to the peak of the third crystal, which remained in place. At the same time, a noticeable increase in the intensity of neutrons reflected from the first crystal is observed.

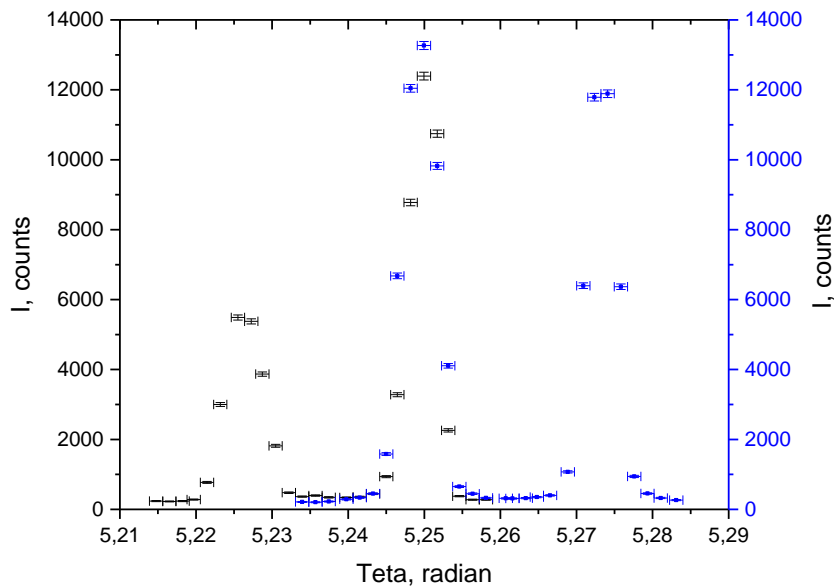


Figure 11. Black points – first crystal with side B23 facing the reactor, then third crystal with side B12. Blue points – third crystal with side A34 facing the reactor, then first with side A23.

From the results, it can be concluded that the holder of the third crystal cannot ensure reliable fixation of two single crystals relative to each other, since orientation effects manifested themselves to a significant extent. It was decided to use another holder with a different system for securing the single crystals.

Figure 12 shows at the top the rocking curve of the corresponding assembly in one position, and at the bottom – after a 180° rotation.

Analyzing the data, it was found that the reflection of the first crystal is shifted relative to the third by approximately 1°21'.

The assembly was then reassembled to check its stability, and the method of fixing the single crystals was changed again, yielding the result shown at the top of Figure 13. The distance between the peak vertices of the rocking curves of the crystals was 23'. Knowing the length of the first crystal and using the relation  $\alpha \approx \sin(\alpha)$ , we found the required shim thickness  $b = \alpha * 34 = 0.2 \text{ mm}$ . Inserting this shim so that the first crystal rotated to the left relative to the reactor, we obtained merged reflections.

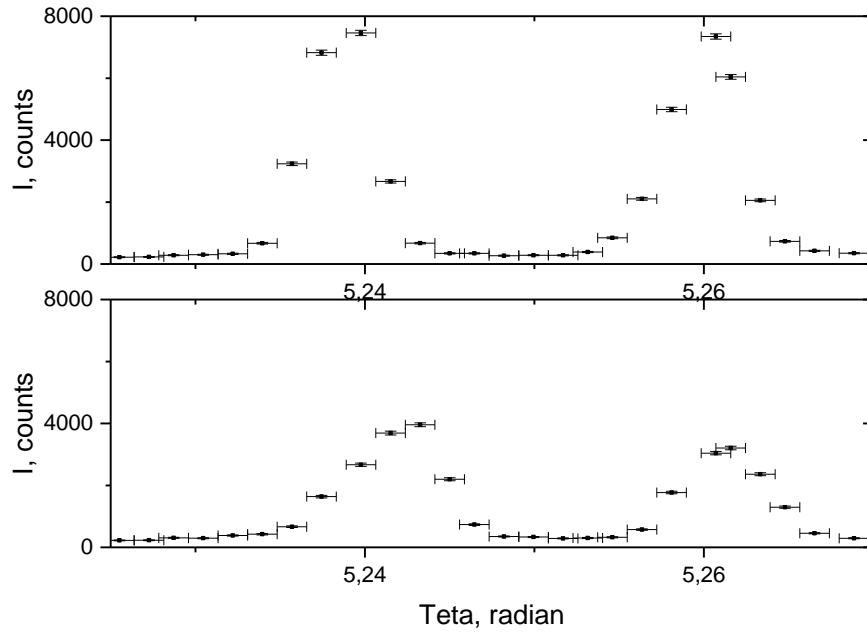


Figure 12. Top graph: third crystal with side A12 facing the reactor, then first with side A41; Bottom graph: first crystal with side B23 facing the reactor, then third with side B12.

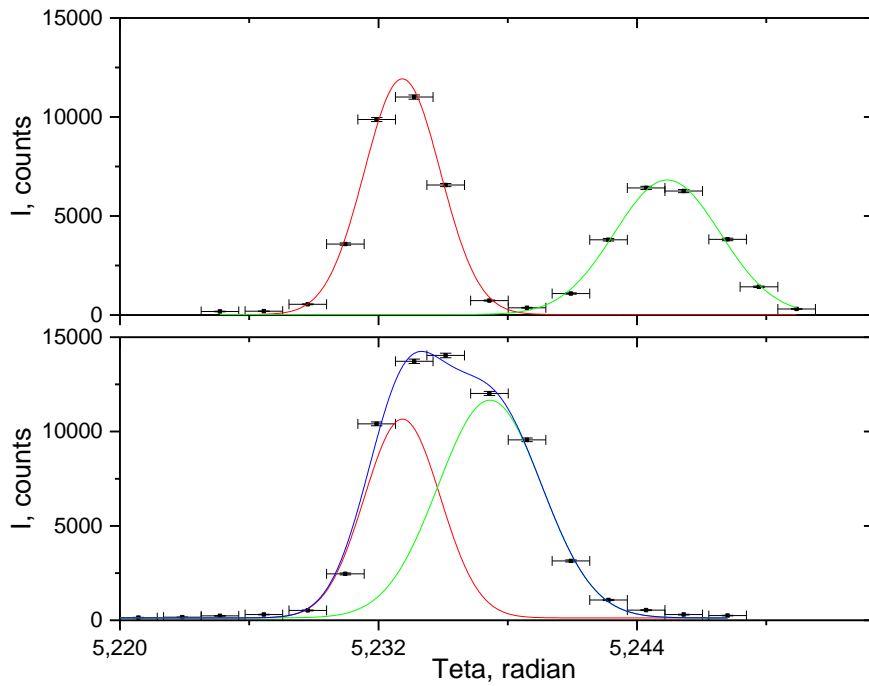


Figure 13. Facing the reactor: third crystal with side A12, first crystal with side A41. Top – without shim, bottom – with shim. The fit for the third crystal is shown in red, the fit for the first in green. The blue line is the total curve.

## 8. Attenuation of the diffracted neutron beam intensity upon passing through a CoFe crystal

Using one of the intermediate assemblies and a fourth CoFe alloy crystal of irregular shape with thickness  $d = 2,6$  mm, the neutron absorption coefficient was determined.

Figure 14 shows the experimental arrangements. In the first measurement, the fourth crystal (hereinafter referred to as the absorber) was absent. In the second measurement, the absorber was placed in the direct neutron beam, partially covering the collimator window opening into the experimental hall. In the third measurement, the absorber was placed in the diffracted beam.

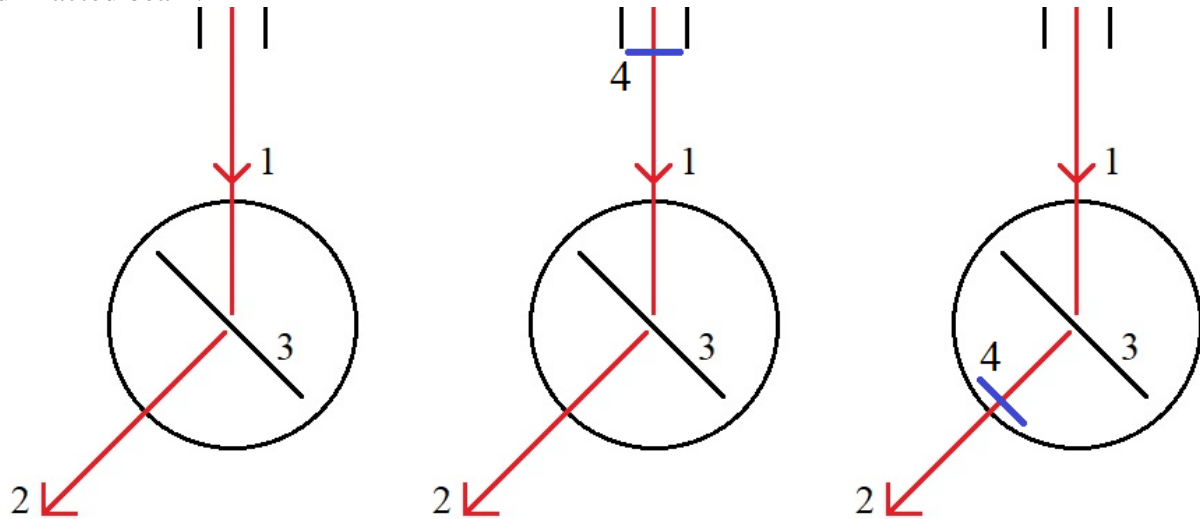


Figure 14. Experimental arrangements. 1 – direct "white" neutron beam, 2 – diffracted neutron beam, 3 – holder with the single-crystal assembly, 4 – absorber crystal.

The measurement time for the time-of-flight spectra for each experiment was 10 minutes. Data acquisition and conversion of the time scale from channels to microseconds were performed using the "Romana" program.

The intensity reduction for the first reflection order was considered. The energy of the diffracted neutrons was found to be  $67.47 \pm 2.73$  meV.

The neutron beam intensity is attenuated according to the formula:

$$I = I_0 \cdot \exp\{-d \cdot \Sigma\}, \quad (8.1)$$

where  $\Sigma$  is the total macroscopic interaction cross-section of neutrons,  $d$  is the thickness of the absorber crystal,  $I_0$  is the integrated intensity of diffracted neutrons in the absence of the absorber, and  $I$  is the integrated intensity of diffracted neutrons with the absorber crystal in the beam. The summation is performed from 6905  $\mu$ s to 8505  $\mu$ s. The results are presented in Table 6.

Table 6. Integrated intensity

Arrangement	I, counts
Absence of the absorber	$125559 \pm 361$
Absorber in direct beam	$99024 \pm 317$
Absorber in diffracted beam	$74640 \pm 278$

Expressing  $\Sigma$  from formula (8.1) we obtained differing results for the two different positions. For the experiment with the absorber in the direct beam  $\Sigma = 0.913 \pm 0,005 \text{ 1/cm}$ . When the fourth crystal was placed in the reflected beam, we obtained  $\Sigma = 2 \pm 0.005 \text{ 1/cm}$

The theoretical value of  $\Sigma$  for the Co(92%)-Fe(8%) alloy is calculated as follows:

$$\Sigma = n_{CoFe} \cdot (0.92\sigma_{Co} + 0.8\sigma_{Fe}), \quad (8.2)$$

where  $\sigma_{Co}$ ,  $\sigma_{Fe}$  are the microscopic cross-sections for the corresponding elements;

$$n_{CoFe} = \frac{N_A \rho_{CoFe}}{A_{CoFe}}, \quad \text{where } N_A \text{ is Avogadro's number, } \rho_{CoFe} \approx 8,13 \frac{g}{cm^3}, \quad A_{CoFe} \approx 58,69 \frac{g}{mol}$$

Natural cobalt consists 100% of the isotope 59, iron has a more complex isotopic composition. Referring to the ENDF library [10] for this neutron energy, the following cross-sections were determined:

Table 7. Isotope microscopic cross-sections of the CoFe alloy

Isotope	Isotopic content, %	Microscopic cross-section, barn
Co-57	100	40.157
Fe-54	5.845	3.549
Fe-56	91.754	13.369
Fe-57	2.119	2.13
Fe-58	0.282	8.3037

Thus, for the calculated value we obtain  $\Sigma = 3.432 \text{ 1/cm}$ .

The discrepancy between the calculated value and the experimental data can be explained by the non-optimal geometry of the experiment.

## Conclusion

As a result of the work carried out, it can be said that a compound neutron polarizer consisting of sequentially arranged single crystals in Laue geometry is not viable. The effects associated with the attenuation of the neutron flux intensity turn out to be stronger than the gain from the crystal mosaicity. Better results could have been achieved by fine-tuning the geometric orientation of the crystals with rotation about all axes, not only about the horizontal axis.

Nevertheless, the work has demonstrated the fundamental possibility of increasing the intensity of polarized neutrons by assembling individual crystals into a stack. The obtained data allow planning the next step, which will be the creation of a polarizer in Bragg geometry. When the crystals are arranged for reflection, the effects associated with neutron extinction will have less influence. Also, the intensity of the diffracted neutron beam will increase due to the larger reflecting surface area.

## Acknowledgements

I would like to express my deepest gratitude to my JINR scientific supervisors Natalia Rebrova and Valery Kuznetsov for many informative discussions and help during the work. I am also grateful to the head of Channel 1 of the IBR reactor, Daniyar Berikov, for providing an internal report and help in tuning the crystal assemblies.

## References

1. Abov, Yu. G., & Krupshitsky, P. A. Parity violation in nuclear interactions. *Physics-Uspekhi* (1976), 118, 141-173. <https://doi.org/10.3367/UFNr.0118.197601d.0141>
2. Abov Yu.G., Alfimenkov V.P., Lason L., Mareev Yu.D., Pikelner L.B., Tsulaia V.M., Tsulaia M.I., Salamatin I.M. – The "Kolchida" Setup for Experimental Studies of Interaction of Polarized Neutrons with Polarized Nuclei [Preprint]. – Dubna: Joint Institute for Nuclear Research, P13-2008-69. – Submitted to Nuclear Instruments and Methods – 25 p.
3. Clark, M. A.; Robson, J. M. A POLARIZED NEUTRON BEAM PRODUCED BY BRAGG REFLECTION FROM CO-Fe ALLOY. *Canadian Journal of Physics* 1961, 39 (1), 1–12. <https://doi.org/10.1139/p61-001>.
4. OriginLab Corporation. Origin — Data Analysis and Graphing Software [Electronic resource]. — URL: <https://www.originlab.com/> (Accessed: February 20, 2026).
5. Wolfram Research, Inc. Wolfram Research — Pushing the Bounds of Technical Computing [Electronic resource]. — URL: <https://www.wolfram.com/> (Accessed: February 20, 2026).
6. Abov, Yu.G., Gulko, A.D., & Krupchinsky, P.A. (1966). Polarized Slow Neutrons. Moscow: Atomizdat. 268 p.
7. Ananiev V. D., Pepelyshev Yu. N., Rogov A. D. Optimization Study of the IBR-2 Reactor // *Physics of Atomic Nuclei*. 2019. T. 82. № 8. C. 1162-1174. <https://doi.org/10.1134/S1063778819080039>.
8. Ananyev V.D., Vinogradov A.V., Dolgikh A.V., Edunov L.V., Pepelyshev Yu.N., Rogov A.D., Tsarenkov S.A., Zaikin A.A., Lokantsev A.A. – Physical Start-up of the Modernized IBR-2 Reactor (IBR-2M). – Dubna: Joint Institute for Nuclear Research, P13-2012-41. – 25 p.
9. Daniyar Berikov, Internal report.
10. Evaluated Nuclear Data File (ENDF) / National Nuclear Data Center (NNDC) // URL: <https://www.nndc.bnl.gov/endl/> (Accessed: March 17, 2026. Requests 79067, 79068, 79069, 79072, 79073).